AIP | Journal of Applied Physics

Magnetic and electrical/thermal transport properties of Mn-doped Mn+1AXn phase compounds Cr2−xMnxGaC (0 ≤ x ≤ 1)

S. Lin, P. Tong, B. S. Wang, Y. N. Huang, W. J. Lu et al.

Citation: J. Appl. Phys. 113, 053502 (2013); doi: 10.1063/1.4789954
View online: http://dx.doi.org/10.1063/1.4789954
View Table of Contents: http://jap.aip.org/resource/1/JAPIAU/v113/i5
Published by the AIP Publishing LLC.

Magnetic and electrical/thermal transport properties of Mn-doped $M_{n+1}AX_n$ phase compounds $Cr_{2-x}Mn_xGaC$ ($0 \le x \le 1$)

S. Lin,[1] P. Tong,[1] B. S. Wang,[1] Y. N. Huang,[1] W. J. Lu,[1] D. F. Shao,[1] B. C. Zhao,[1] W. H. Song,[1] and Y. P. Sun[1,2,a)]
[1]*Key Laboratory of Materials Physics, Institute of Solid State Physics, Hefei 230031, People's Republic of China*
[2]*High Magnetic Field Laboratory, Chinese Academy of Sciences, Hefei 230031, People's Republic of China*

(Received 21 September 2012; accepted 15 January 2013; published online 1 February 2013)

In this paper, we report the effects of partial substitution of Mn for Cr on the structural, magnetic, and electrical/thermal transport properties of $M_{n+1}AX_n$ phase compounds $Cr_{2-x}Mn_xGaC$ ($0 \le x \le 1$). As a result, the unit cell volume and the thermal conductivity decrease while the resistivity increases with increasing x. Interestingly, the magnetism of $Cr_{2-x}Mn_xGaC$ changes from the nonmagnetic Cr_2GaC ($x = 0$) to the ferrimagnetic CrMnGaC ($x = 1$). In order to shed light on the discrepancy observed between Hall coefficient and Seebeck coefficient of Cr_2GaC, the electrical conductivity, Hall coefficient, and magnetoresistance are analyzed within a two-band model. Furthermore, an upturn is observed in low-temperature specific heat of $Cr_{2-x}Mn_xGaC$, which may be related with the magnetic Mn dopant. © *2013 American Institute of Physics*. [http://dx.doi.org/10.1063/1.4789954]

I. INTRODUCTION

Recently, the layered ternary carbides and nitrides [with the general chemical formula $M_{n+1}AX_n$ (MAX), where n = 1, 2, 3, M is an early transition metal, A is an A element (mostly IIIA and IVA), and X is either C or N][1] have attracted considerable attention owing to their interesting physical and mechanical properties, viz. electrically and thermally conductive, elastically stiff as well as lightweight.[2–14] Moreover, the MAX phase compounds are resistant to thermal shock and unusually damage tolerant. As a typical MAX phase compound Cr_2GaC (to see Fig. 1, where shows the crystal structure of Cr_2GaC), it has been prepared successfully for several decades, but little attention has been paid. Very recently, the single crystal of Cr_2GaC has been grown and the bulk moduli of Cr_2GaC under high pressure (50 GPa) have also been investigated.[15,16] However, little is known about the evolution of physical properties as a function of chemical doping in Cr_2GaC. As reported in previous investigations, the chemical ratio of Si/Ge could availably manipulate the basic physical properties (e.g., electronic, thermal, and elastic properties) of MAX phase $Ti_3Si_{1-x}Ge_xC_2$.[17] Their experimental results indicated that the distance of MX-A-MX layers is a pivotal element to determine the physical properties. Analogously, the chemical doping may also affect the basic physical properties of isostructural Cr_2GaC. Besides, previous investigations indicate that the MAX phase compounds are almost non-magnetism and the detailed origin is unclear up to now. However, in Mn-doped MAX phase compounds $Cr_{2-x}Mn_xAlC$ alloys, the stable magnetic phase starts to exist with increasing Mn doping level while the micromechanism is unknown.[18] Therefore, the study of Mn-doped MAX phase compound Cr_2GaC may be of great importance and helpful to understood the magnetic interactions and the evolution of physical properties.

In this work, we have investigated the effects of Mn doping on the structural, magnetic, and electrical/thermal transport properties in $Cr_{2-x}Mn_xGaC$. As a result, the unit cell volume and the thermal conductivity decrease while the magnitude of resistivity increases with increasing x. Interestingly, the magnetism changes from the nonmagnetic Cr_2GaC ($x = 0$) to the ferrimagnetic CrMnGaC ($x = 1$).

II. EXPERIMENTAL DETAILS

Polycrystalline samples $Cr_{2-x}Mn_xGaC$ ($0 \le x \le 1$) were prepared by the direct reaction of the constituent elements of gallium (3 N), chromium (3 N), graphite (3 N), and manganese (3 N). The starting materials were mixed in the desired proportions, sealed in evacuated quartz tubes (10^{-3} Pa), and then annealed at 1123–1173 K for about five days. After quenching the tubes to room temperature, the products were pulverized, mixed, pressed into pellets (15 MPa), and annealed at 1273 K for about eight days in order to obtain the homogeneous samples. Powder X-ray diffraction (XRD) studies were carried out around room temperature using an X-ray diffractometer with Cu K_α radiation (PHILIPS, $\lambda = 0.15406$ nm) to determine the crystal structure and phase purity. Magnetic measurements were performed on a Quantum Design superconducting quantum interference device magnetometer (SQUID 5 T). The electrical transport properties were measured on a Quantum Design physical property measurement system (PPMS 9 T). The electrical transport properties were measured by the standard four-probe method to eliminate contact resistance for these low resistivity materials. The Hall measurements were performed by using five-probe method on PPMS 9 T. The Seebeck coefficient and thermal conductivity were also measured on PPMS 9 T.

a)Author to whom correspondence should be addressed. Electronic mail: ypsun@issp.ac.cn. Tel.: +86-551-559-2757. Fax: +86-551-559-1434.

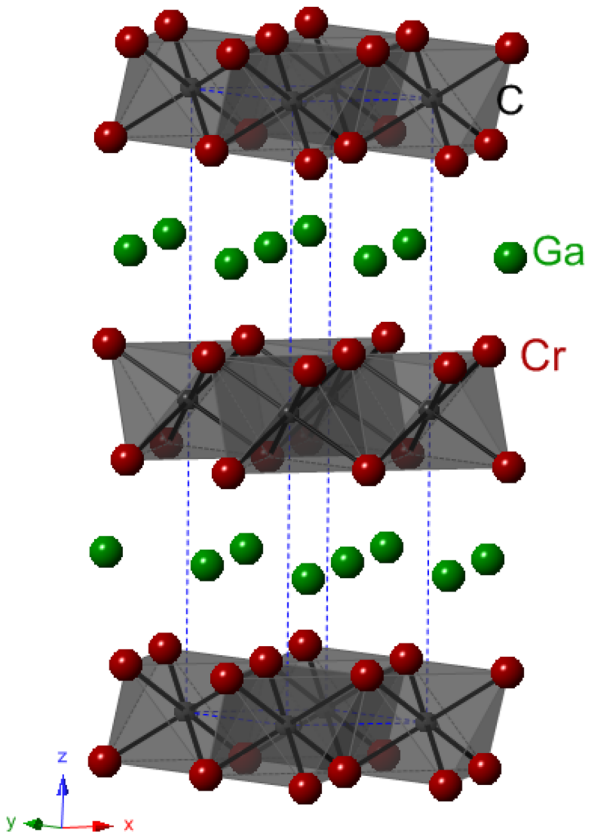

FIG. 1. Crystal structure of Cr_2GaC.

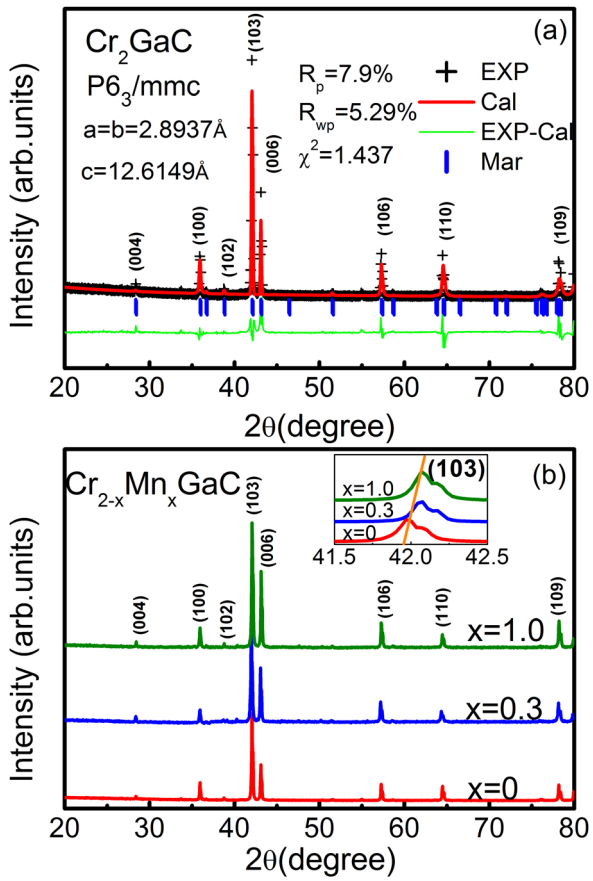

FIG. 2. (a) The Rietveld refined powder XRD pattern for parent compound Cr_2GaC; The vertical marks (blue line) indicate the position of Bragg peaks, and the solid line (green line) at the bottom corresponding to the difference between experimental and calculated intensities. (b) Room-temperature X-ray powder diffractions for all the samples $Cr_{2-x}Mn_xGaC$ ($0 \le x \le 1.0$); Inset shows the enlargement of XRD diffraction peak (103) for $Cr_{2-x}Mn_xGaC$ ($0 \le x \le 1.0$).

III. RESULTS AND DISCUSSION

In order to investigate the compactness of our samples synthesized by aforementioned method, the density of our samples was measured. As a result, the density of Cr_2GaC (6.68 g/cm^3) is almost consistent with the calculated value (6.7 g/cm^3) reported previously,[15] and the densities of $Cr_{1.7}Mn_{0.3}GaC$ and CrMnGaC are 6.67 g/cm^3 and 6.63 g/cm^3, respectively. Considering the experimental errors, our samples are almost fully dense.

Figure 2(a) shows the Rietveld refined powder XRD patterns for parent compound Cr_2GaC. The related fitting parameter values (such as χ^2, R_p, and R_{wp}) are considerable low as presented, indicating that the sample is good in quality. The refined lattice constants $a = b = 2.8937$ Å and $c = 12.6149$ Å for Cr_2GaC, which are very close to the values reported previously.[15] Fig. 2(b) displays the room-temperature XRD patterns for all the samples of $Cr_{2-x}Mn_xGaC$. Obviously, all the samples are single-phase (space group: $P6_3/mmc$) without any impurities. It is necessary to point that the samples with high doping level ($x = 1.5$, 2.0) synthesized in the same batch have plenty of impurities (C and Mn_3GaC). The inset of Fig. 2(b) presents the enlargement of XRD diffraction peak (103), which moves to high angles with increasing x, meaning a successful Mn doping in $Cr_{2-x}Mn_xGaC$. According to the results of Rietveld refinements for $Cr_{2-x}Mn_xGaC$, we find that the unit cell volume decreases with increasing x, which may be related with the smaller atom radius of Mn compared with that of Cr.

To date, and to the best of our knowledge, there is little report about the magnetism of MAX phase compounds. As reported by Dahlqvist *et al.*, the MAX phase compound Cr_2AlC is nonmagnetic.[18] Analogously, the isostructural Cr_2GaC is nonmagnetic. In order to investigate the effect of Mn doping on the magnetism of $Cr_{2-x}Mn_xGaC$, we measured the temperature dependent magnetization $M(T)$ and the isothermal magnetic hysteresis loop $M(H)$ for the selected sample CrMnGaC. Figure 3(a) depicts $M(T)$ curves for the sample CrMnGaC at a magnetic field of $(10^6/4\pi)$ A/m under zero-field-cooled (ZFC) measuring mode. The $M(T)$ curve shows that the magnetization increases significantly with decreasing temperature, which indicates a paramagnetic behavior. The inset of Fig. 3(a) presents the temperature dependence of the inverse of magnetic susceptibility $\chi^{-1}(T)$ curve. Between $T = 200$ and 350 K, $\chi^{-1}(T)$ is proportional to temperature manifesting a Curie-Weiss behavior. We obtained the effective moment $\mu_{eff} = 1.632\,\mu_B$ and the corresponding Weiss-temperature is -652.5 K for CrMnGaC. Fig. 3(b) displays the isothermal $M(H)$ at 5 K, which increases in an essentially linear fashion with magnetic field. However, there exists a tiny anomaly around low magnetic field, indicating that there exists a weak ferrimagnetism at the ground state.

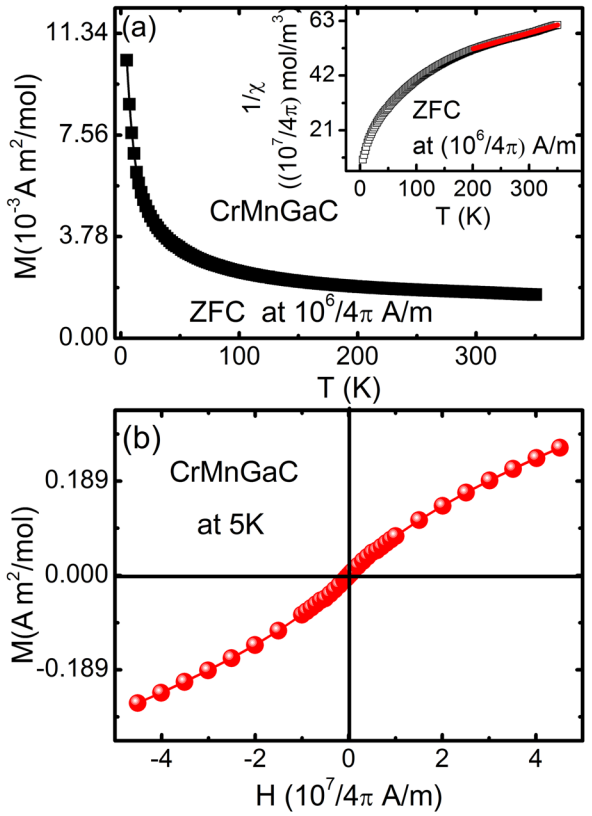

FIG. 3. (a) Temperature dependent magnetization $M(T)$ curves for the sample CrMnGaC at a magnetic field of $(10^6/4\pi)$ A/m under ZFC; The inset displays the temperature dependent inverse magnetic susceptibility $\chi^{-1}(T)$ for CrMnGaC at a magnetic field of $(10^6/4\pi)$ A/m under ZFC. (b) The isothermal $M(H)$ at 5 K for CrMnGaC.

Figure 4(a) presents the temperature dependent resistivity $\rho(T)$ curves for $Cr_{2-x}Mn_xGaC$ at zero magnetic field between 2 and 350 K. All the samples' resistivity curves show a metallic behavior, i.e., the magnitude of resistivity decreases with decreasing temperature.[17,19–21] The low-temperature residual resistivity and the residual resistivity ratio (RRR), defined as $RRR = \rho(300\,K)/\rho(5\,K)$, are measures of sample quality such as in metals and alloys. High residual resistivity values and small RRRs suggest sizable scattering from impurities, vacancies, or other defects. As shown in Fig. 4(a), the residual resistivity increases with doping level x in $Cr_{2-x}Mn_xGaC$. Moreover, the RRR decreases with increasing x shown in inset of Fig. 4(a). Especially, Cr_2GaC has the largest RRR of 47.8, indicating a good quality of the sample. All these results can be understood as follows: As the doping level x increasing, more and more Mn atoms enter into the site of Cr and the sizes of both atoms are different, resulting in an increase of lattice disorder. As a result, the resistivity increases while the RRR decreases with increasing x. Fig. 4(b) shows the resistivity at zero magnetic field and $(5 \times 10^7/4\pi)$ A/m from 5 to 350 K for the selected samples (Cr_2GaC and CrMnGaC). Obviously, the curves between zero magnetic field and $(5 \times 10^7/4\pi)$ A/m are almost overlapped for both selected samples, indicating that the magnetoresistance (MR), defined as $MR = [\rho(H) - \rho(0)]/\rho(0)$, is considerable small. To further study the electronic transport mechanism, the low-temperature (2–70 K) resistivity data of $Cr_{2-x}Mn_xGaC$ are fitted by the following formula:

$$\rho(T) = \rho_0 + AT^{\delta}, \tag{1}$$

where ρ_0 and A represent the residual resistivity and T^{δ} term coefficient of the resistivity, respectively; δ is the exponent (to see Fig. 4(c)). The x dependence of fitting parameter δ is plotted in inset of Fig. 4(c). Obviously, the magnitude of δ is changed with x. Interestingly, no $\delta = 2$ is observed, meaning that the carrier transport of samples with $x = 0$, 0.3, and 1.0 may behave as a non-Fermi-liquid behavior at low temperatures. However, it is found that the δ decreases from 2.5 to 1.2

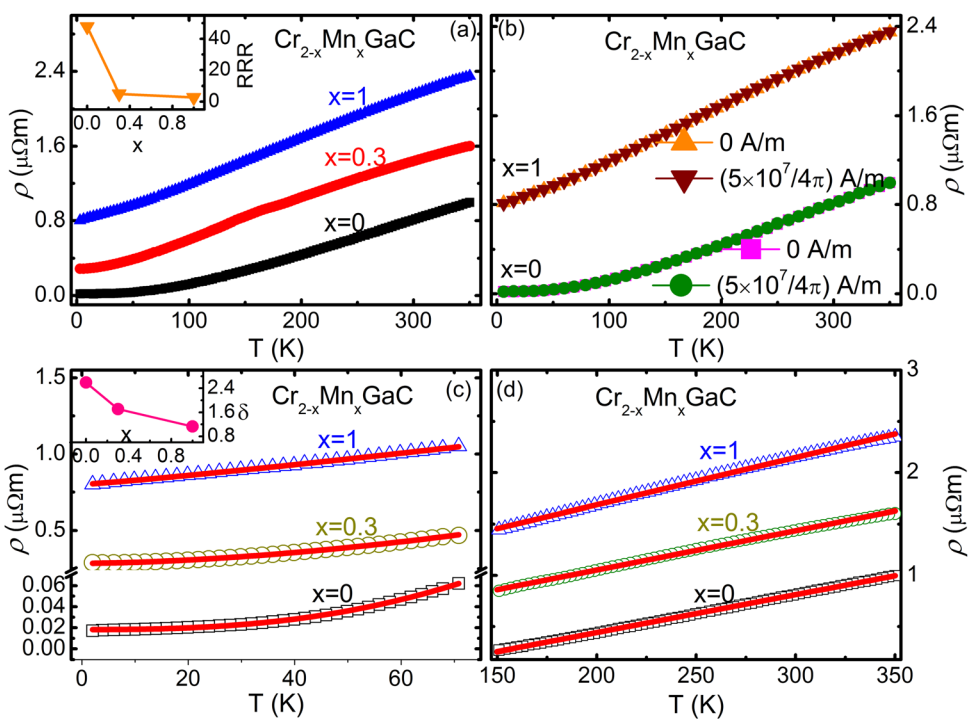

FIG. 4. (a) Temperature dependent resistivity ρ(T) curves measured at zero magnetic field from 2 to 350 K; Inset shows the doping level x dependence of RRR value. (b) Temperature dependent resistivity ρ at zero magnetic field and $(5 \times 10^7/4\pi)$ A/m for the samples with $x = 0$ and $x = 1.0$, respectively. (c) The solid lines represent the fitting results according to Eq. (1); Inset displays the fitting parameter δ as a function of doping level x. (d) Linear fits of $\rho(T)$ data for all the samples $Cr_{2-x}Mn_xGaC$ ($0 \le x \le 1.0$) between 150 and 350 K; Solid lines are fitting results. Inset presents the fitting slopes as a function of doping level x.

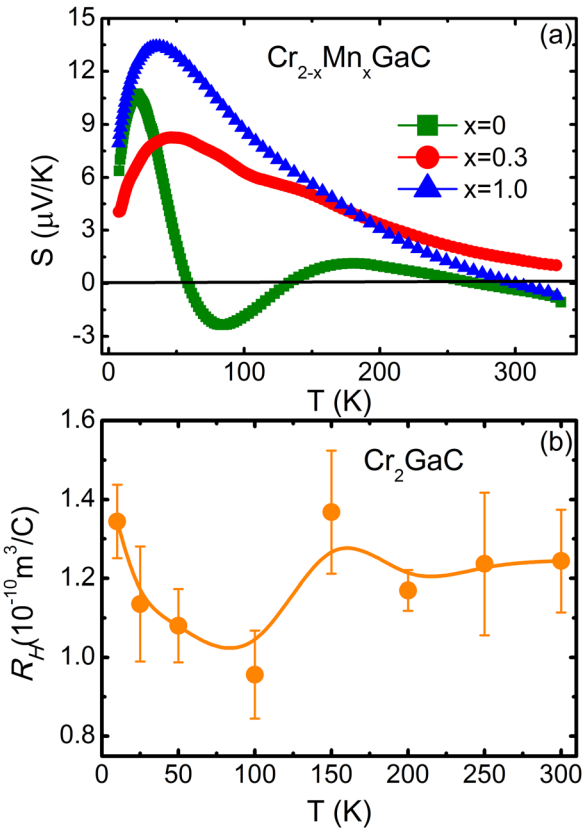

FIG. 5. (a) Temperature dependent Seebeck coefficient at zero magnetic field between 5 and 330 K for $Cr_{2-x}Mn_xGaC$. (b) Temperature dependent the Hall coefficient for Cr_2GaC.

with increasing x. That is to say, it would be possible that there exists $\delta = 2$ if a suitable x value was selected. Meanwhile, at the elevated temperatures (150–350 K), $\rho(T)$ increases linearly with increasing the temperature for all the samples according to the fitting results (to see Fig. 4(d)), indicating that the contribution of electron-phonon scatterings is dominant.[22] This behavior can be simply understood as follows: With increasing the temperature, the number of phonon increases quickly, resulting in the enhancement of the phonon scatterings.

Figure 5(a) shows the temperature dependent Seebeck coefficient $S(T)$ for $Cr_{2-x}Mn_xGaC$ between 5 and 330 K. Generally, the sign of $S(T)$ is often used to qualitatively determine the type of the dominant charge carrier. Obviously, the $S(T)$ values of the samples with $x = 0.3$ and 1.0 are positive, which increase firstly and then decrease around 50 K with decreasing temperature. However, the $S(T)$ value of Cr_2GaC is small and fluctuates around zero from 330 to 50 K and then becomes positive totally below 50 K. Meanwhile, Fig. 5(b) displays the temperature dependent R_H for Cr_2GaC. Obviously, the R_H is positive in the whole temperature range (300-5 K), indicating that the dominant carriers are hole-type. The divergence in S(T) and R_H(T) suggests that in Cr_2GaC two-band model should be considered to explain the above results. Within a two-band framework, the R_H is described according to the following formula:

$$R_H = \frac{(\mu_p^2 p - \mu_n^2 n)}{e(\mu_p p + \mu_n n)^2}. \quad (2)$$

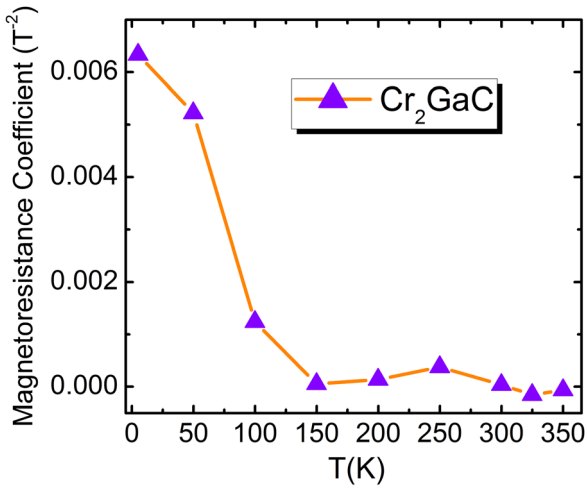

FIG. 6. Temperature dependence of the magnetoresistance coefficient α for Cr_2GaC.

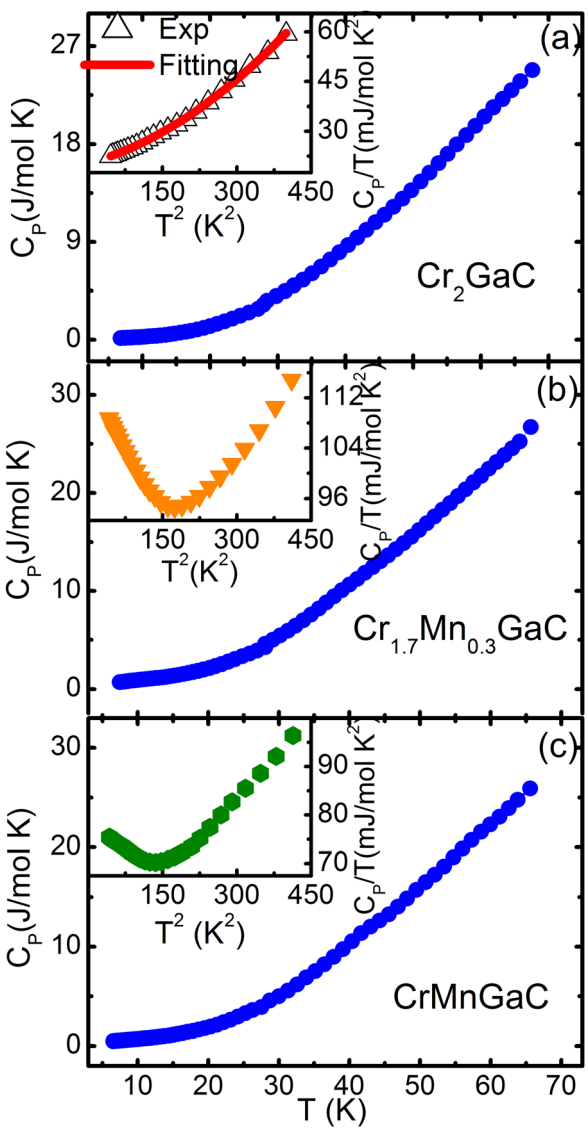

FIG. 7. (a)-(c) Temperature dependent heat capacity $C_P(T)$ at zero field in a temperature of 6.5-65 K for $Cr_{2-x}Mn_xGaC$; Inset shows the plot of $C_P(T)/T$ vs. T^2 below 20 K and the solid line represents the fitting results according to Eq. (6).

This expression contains four unknown parameters: μ_p, μ_n, p, and n which are the hole and electron mobilities and the hole and electron concentrations, respectively. To solve completely for each unknown parameter, three additional constraints are required. In the two-band model, the $MR = [\rho(H) - \rho(0)]/\rho(0) = \Delta\rho/\rho$ and the electrical conductivity σ are described by

$$\frac{\Delta\rho}{\rho} = \alpha B^2 = \frac{\mu_n\mu_p np(\mu_n + \mu_p)^2}{(n\mu_n + p\mu_p)^2}B^2, \quad (3)$$

$$\sigma = \frac{1}{\rho} = e(n\mu_n + p\mu_p). \quad (4)$$

Based on previous work,[19,23] we assume that $\mu_p = \mu_n$. A major advantage of this approach is its simplicity. And then Eq. (3) degenerates to

$$\mu_p = \mu_n = \sqrt{\alpha}. \quad (5)$$

Figure 6 shows the temperature dependence of magnetoresistance coefficient α for Cr_2GaC, and the $\alpha = 1 \times 10^{-4}$ m^4/V^2s^2 and 6.4×10^{-3} m^4/V^2s^2 around 300 K and 5 K, respectively. Correspondingly, using Eq. (5), we obtain the $\mu_p = \mu_n = 0.01$ m^2/V s around 300 K and $\mu_p = \mu_n = 0.08$ m^2/V s at 5 K. Once the mobilities are determined, their values are inserted in Eqs. (2) and (4). As a result, n and p are estimated to be $p = 1.80 \times 10^{27}$ m^{-3} and $n = 1.60 \times 10^{27}$ m^{-3} around 300 K and $p = 1.91 \times 10^{27}$ m^{-3} and $n = 1.65 \times 10^{27}$ m^{-3} at 5 K for Cr_2GaC. These values are comparable with those of isostructural Cr_2AlC and Ti_2AlC reported previously.[23]

Figures 7(a)–7(c) show the specific heat $C_P(T)$ for $Cr_{2-x}Mn_x$ GaC ($x = 0$, 0.3, and 1.0) measured between 6.5 and 65 K at zero field. As shown in the inset of Fig. 7(a), the data below 20 K are plotted as $C_P(T)/T$ vs. T^2 which can be well expressed by using the following equation:[24]

$$C_P(T)/T = \gamma + \beta T^2 + \delta T^4, \quad (6)$$

where γ (Sommerfeld constant) is the electronic contribution, β is the phonon contribution, and δ is deviations from the linear dispersion of the acoustic modes in extended temperature range. The fitted values of parameters γ, β, and δ are 20.25 mJ/(mol K^2), 0.042 mJ/(mol K^4), and 1.41×10^{-4} mJ/(mol K^6), respectively. Accordingly, the Debye temperature $\Theta_D = \left(\frac{N \times 1.94 \times 10^6}{\beta}\right)^{1/3} = 569$ K (where N is the number of atoms in a unit cell and equal to 4 for Cr_2GaC) is derived from the value of coefficient β. For the Mn-doped samples, the data below 20 K are also plotted as $C_P(T)/T$ vs. T^2, which are shown in insets of Figs. 7(b) and 7(c). Obviously, in the low temperature, there exists an upturn in both insets of Figs. 7(b) and 7(c). As reported by Lue *et al.*,[25] there exists an upturn in specific heat at low temperatures, which is attributed to magnetic defects caused by the Fe antisite defects in nonmagnetic Fe_2VAl. Similarly, it is suggested that the observed low temperature upturn phenomenon in specific heat curve may originate from the magnetic defects due to the magnetic Mn dopant in nonmagnetic Cr_2GaC. However, the detailed origins of low-T specific heat upturn need further experimental and theoretical studies.

Figure 8(a) displays the temperature dependent thermal conductivity $k(T)$ for $Cr_{2-x}Mn_xGaC$ ($0 \le x \le 1.0$) at zero field (5-330 K). Obviously, the thermal conductivity of Cr_2GaC is larger than those of $Cr_{1.7}Mn_{0.3}GaC$ and CrMnGaC. The large thermal conductivity (35 W/m K around 45 K) of Cr_2GaC is comparable with other MAX phase compounds such as Ti_2AlC (about 34 W/m K around 300 K),[23] V_2AlC (about 48 W/m K around 50 K),[23] Ti_3AlC_2

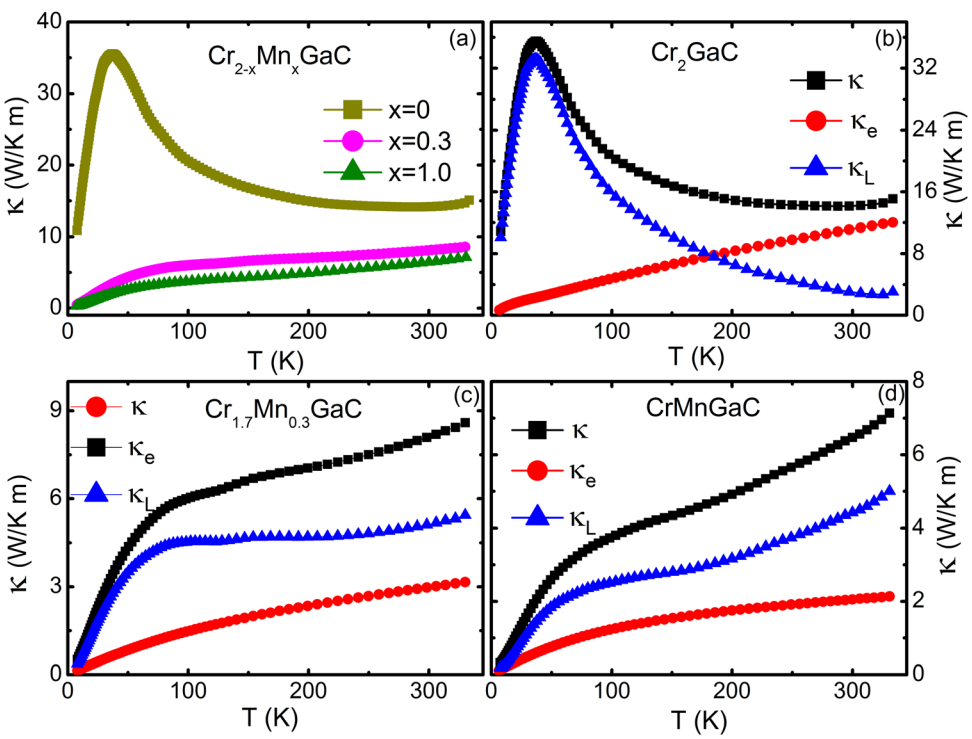

FIG. 8. (a) Temperature dependent thermal conductivity $k(T)$ for $Cr_{2-x}Mn_xGaC$ between 5 and 330 K. (b)–(d) Temperature dependent thermal conductivity $k(T)$, electronic thermal conductivity κ_e, lattice thermal conductivity κ_L for $Cr_{2-x}Mn_xGaC$ at zero field (5-330 K).

(about 38 W/m K around 70 K),[19] which is in agreement with the fact that the MAX phase compounds are good thermal conductors. Generally, the total thermal conductivity can be expressed as a sum of lattice (κ_L) and electronic (κ_e) terms, i.e., $\kappa(T) = \kappa_L(T) + \kappa_e(T)$. The electronic thermal conductivity κ_e can be estimated based on the Wiedemann-Franz (WF) law [$\kappa_e\rho/T = L_0$, where $L_0 = 2.45 \times 10^{-8}\text{W}\Omega\text{K}^{-2}$ is the Lorentz number] and the value of κ_L was obtained in terms of $\kappa(T) - \kappa_e(T)$. Previous experimental investigations have approved that the WF law is an universal formula for many materials [including simple metals, strongly electron-correlated compounds, and low-dimensional systems].[26,27] In this work, the values of κ_L and κ_e were separated and plotted as a function of temperature in Figs. 8(b)–8(d). Obviously, for Cr_2GaC, the value of κ_L is much larger than that of κ_e at low temperature, indicating that the total $\kappa(T)$ mainly originates from the contribution of κ_L spanning the temperature range (5-150 K). Accordingly, the broadened peak of $\kappa(T)$ around 50 K can be also attributed to T-dependent value of κ_L. For the doped samples $Cr_{1.7}Mn_{0.3}GaC$ and CrMnGaC, the value of κ_L is larger than that of κ_e, indicating that the lattice thermal conductivity is dominant in whole temperature range (5-330 K).

In summary, we investigated the effects of the Mn doping on the structural, magnetic, and electrical/thermal transport properties in MAX phase compounds $Cr_{2-x}Mn_xGaC$ ($0 \leq x \leq 1.0$). With increasing x the unit cell volume and the thermal conductivity decrease while the resistivity increases. Interestingly, the magnetism is introduced by the Mn doping at Cr sites in $Cr_{2-x}Mn_xGaC$ ($0 \leq x \leq 1.0$), and the ferrimagnetism for the sample CrMnGaC ($x = 1$) is observed. The electrical conductivity, R_H, and *MR* for Cr_2GaC are analyzed within a two-band model, and the carrier concentrations are $p = 1.80 \times 10^{27}\,\text{m}^{-3}$ and $n = 1.60 \times 10^{27}\,\text{m}^{-3}$ around 300 K and $p = 1.91 \times 10^{27}\,\text{m}^{-3}$ and $n = 1.65 \times 10^{27}\,\text{m}^{-3}$ at 5 K. Furthermore, we also measure the specific heat of $Cr_{2-x}Mn_xGaC$ and observe that there is an upturn in low-temperature specific heat curve in Mn-doped samples, which may be related to the Mn dopant. It is noteworthy that the thermal conductivity is also high up to 35 W/m K around 45 K for Cr_2GaC.

ACKNOWLEDGMENTS

This work was supported by the National Key Basic Research under Contract No. 2011CBA00111 and the National Natural Science Foundation of China under Contract Nos. 51001094, 51171177, 11174295, U1232139, and Director's Fund of Hefei Institutes of Physical Science, Chinese Academy of Sciences.

[1]H. Nowotny, Prog. Solid State Chem. **5**, 27 (1970).
[2]M. W. Barsoum and T. El-Raghy, J. Am. Ceram. Soc. **79**, 1953 (1996).
[3]M. W. Barsoum, D. Brodkin, and T. El-Raghy, Scr. Mater. **36**, 535 (1997).
[4]M. W. Barsoum, Prog. Solid State Chem. **28**, 201 (2000).
[5]M. W. Barsoum, L. Farber, T. El-Raghy, and I. Levin, Metall. Mater. Trans. A **30**, 1727 (1999).
[6]J. C. Ho, H. H. Hamdeh, M. W. Barsoum, and T. El-Raghy, J. Appl. Phys. **86**, 3609 (1999).
[7]R. Pampuch, J. Lis, L. Stobierski, and M. Tymkiewicz, J. Eur. Ceram. Soc. **5**, 283 (1989).
[8]M. W. Barsoum, L. Farber, I. Levin, A. Procopio, T. El-Raghy, and A. Berner, J. Am. Ceram. Soc. **82**, 2545 (1999).
[9]M. W. Barsoum and T. El-Raghy, Metall. Mater. Trans. A **30**, 363 (1999).
[10]N. Tzenov and M. W. Barsoum, J. Am. Ceram. Soc. **83**, 825 (2000).
[11]M. W. Barsoum, T. El-Raghy, and A. Procopio, Metall. Mater. Trans. A **31**, 373 (2000).
[12]M. W. Barsoum, H.-I. Yoo, I. K. Polushina, Yu. V. Rud, and T. El-Raghy, Phys. Rev. B **62**, 10194 (2000).
[13]P. Finkel, M. W. Barsoum, and T. El-Raghy, J. Appl. Phys. **87**, 1701 (2000).
[14]H.-I. Yoo, M. W. Barsoum, and T. El-Raghy, Nature (London) **407**, 581 (2000).
[15]J. Etzkorn, M. Ade, D. Kotzott, M. Kleczek, and H. Hillebrecht, Solid State Chem. **182**, 995 (2009).
[16]B. Manoun, S. Kulkarni, N. Pathak, S. K. Saxena, S. Amini, and M. W. Barsoum, J. Alloys Compd. **505**, 328 (2010).
[17]P. Finkel, B. Seaman, K. Harrell, J. Palma, J. D. Hettinger, and S. E. Lofland, Phys. Rev. B **70**, 085104 (2004).
[18]M. Dahlqvist, B. Alling, I. A. Abrikosov, and J. Rosen, Phys. Rev. B **84**, 220403(R) (2011).
[19]J. D. Hettinger, S. E. Lofland, P. Finkel, T. Meehan, J. Palma, K. Harrell, S. Gupta, A. Ganguly, T. El-Raghy, and M. W. Barsoum, Phys. Rev. B **72**, 115120 (2005).
[20]T. H. Scabarozi, S. Amini, P. Finkel, O. D. Leaffer, J. E. Spanier, M. W. Barsoum, M. Drulis, H. Drulis, W. M. Tambussi, J. D. Hettinger, and S. E. Lofland, J. Appl. Phys. **104**, 033502 (2008).
[21]P. Finkel, J. D. Hettinger, S. E. Lofland, M. W. Barsoum, and T. El-Raghy, Phys. Rev. B **65**, 035113 (2001).
[22]P. Tong, Y. P. Sun, B. C. Zhao, X. B. Zhu, and W. H. Song, Solid State Commun. **138**, 64 (2006).
[23]T. Scabarozi, A. Ganguly, J. D. Hettinger, S. E. Lofland, S. Amini, P. Finkel, T. El-Raghy, and M. W. Barsoum, J. Appl. Phys. **104**, 073713 (2008).
[24]P. Tong, Y. P. Sun, X. B. Zhu, and W. H. Song, Phys. Rev. B **74**, 224416 (2006).
[25]C. S. Lue, J. H. Ross, Jr., C. F. Chang, and H. D. Yang, Phys. Rev. B **60**, R13941 (1999).
[26]S. Y. Li, L. Taillefer, D. G. Hawthorn, M. A. Tanatar, J. Paglione, M. Sutherland, R. W. Hill, C. H. Wang, and X. H. Chen, Phys. Rev. Lett. **93**, 056401 (2004).
[27]R. W. Hill, G. Proust, L. Taillefer, P. Fournier, and R. L. Greene, Nature (London) **414**, 711 (2001).